5th GRACM International Congress on Computational Mechanics
Limassol, 29 June – 1 July, 2005

COHESIVE MODELING OF PROPAGATING CRACKS IN HOMOGENEOUS AND FUNCTIONALLY GRADED COMPOSITES

Glaucio H. Paulino* **and Zhengyu Zhang**

Department of Civil and Environmental Engineering, University of Illinois at Urbana-Champaign, Newmark Laboratory, 205 North Mathews Avenue, Urbana, IL 61801, U.S.A.

*e-mail:paulino@uiuc.edu, web page: http://www.cee.uiuc.edu/paulino

Keywords: Finite element method, functionally graded material (FGM), cohesive zone model (CZM), dynamics, crack, fracture.

Abstract. *This paper presents a Cohesive Zone Model (CZM) approach for investigating dynamic crack propagation in homogeneous and Functionally Graded Materials (FGMs). The failure criterion is incorporated in the CZM using both a finite cohesive strength and work to fracture in the material description. A novel CZM for FGMs is explored and incorporated into a finite element framework. The material gradation is approximated at the element level using a graded element formulation. A numerical example is provided to demonstrate the efficacy of the CZM approach, in which the influence of the material gradation on the crack branching pattern is studied.*

1 INTRODUCTION

Functionally graded materials or FGMs are a new generation of engineered composites characterized by spatially varied microstructures and smooth variation of mechanical/thermal/electromagnetic properties. This new concept of engineering the material microstructure and recent advances in material processing science allows one to fully integrate the desirable properties of individual material phases and acquire optimized structural performance[1].

Fracture mechanics of FGMs has been an active area of research during recent years[2]. Compared to the classical linear elastic fracture mechanics (LEFM) and some other existing fracture models, Cohesive Zone Models (CZMs) provide advantages of allowing spontaneous crack nucleation, crack branching and fragmentation, as well as crack propagation without an external fracture criterion[3, 4].

CZMs incorporate a cohesive strength and finite work to fracture in the description of material behavior, and allow simulation of near-tip behavior and crack propagation. The concept of "cohesive failure" is illustrated in Figure 1, in which a *cohesive zone*, along the plane of potential crack propagation, is present in front of the crack tip. Within the extent of the cohesive zone, the material points which were identical when the material was intact, separate to a distance Δ due to influence of high stress state at the crack tip vicinity. The cohesive zone surface sustains a distribution of tractions T which are function of the displacement jump across the surface Δ, and the relationship between the traction T and separation Δ is defined as the constitutive law for the cohesive zone surface.

CZMs can be categorized into two major groups: intrinsic CZMs and extrinsic CZMs. Brief discussion on the characteristics of each will be presented in Section 3. For intrinsic CZM as employed in this numerical example, the traction T first increases with increasing interfacial separation Δ, reaches a maximum value δ, then decreases and finally vanishes at a characteristic separation value δ_c, where complete decohesion is assumed to occur.

The CZM approach has the promise of simulating fracture process where cracking occurs spontaneously. The fracture path and speed become natural outcome of the simulation rather than being specified *ad hoc* or *a priori*. In this paper, a novel cohesive zone model developed for FGMs[6] is adopted to simulate dynamic crack growth in FGMs.

2 NUMERICAL SCHEME

This section briefly outlines the essential components of the numerical scheme, namely, the FEM framework incorporating CZM, the dynamic updating scheme and the material gradation.

To incorporate a CZM into the numerical scheme for dynamic fracture, the *cohesive element* is developed and positioned along the potential path or region of crack propagation, and attached to the volumetric elements, which follows a cohesive *traction-separation* relationship as shown in Figure 1. In

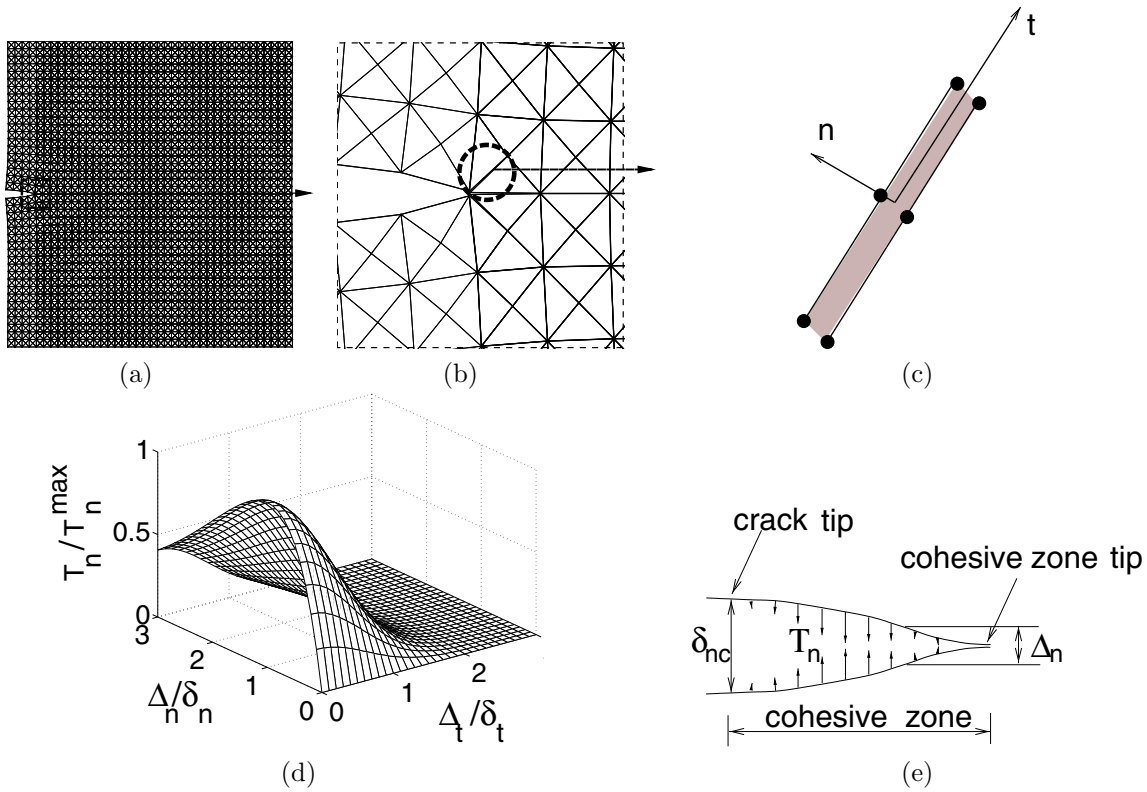

Fig. 1: Schematic representation of cohesive zone model concept; (a) A plate containing crack; At potential crack propagation path *e.g.*, as circled in (b), cohesive element is inserted, as shown in (c), which follows the specified cohesive zone model shown in (d) for normal traction; (e) cohesive zone in Mode I case.

contrast, the conventional finite element, which is now called "*bulk* element", follows conventional *stress-strain* relationships (continuum description). The constitutive law of cohesive elements is inherently embedded in the finite element model, so that the presence of cohesive elements allows spontaneous crack propagation.

The FEM formulation incorporating cohesive elements is derived from the principle of virtual work, and discretized using the explicit central difference time stepping scheme to update displacements $\mathbf{u}$, accelerations $\ddot{\mathbf{u}}$ and velocities $\dot{\mathbf{u}}$ as follows:

$$\mathbf{u}_{n+1} = \mathbf{u}_n + \Delta t \dot{\mathbf{u}}_n + \frac{1}{2}(\Delta t)^2 \ddot{\mathbf{u}}_n \tag{1}$$

$$\ddot{\mathbf{u}}_{n+1} = \mathbf{M}^{-1}(\mathbf{F} - \mathbf{R}_{int_{(n+1)}}) + \mathbf{R}_{coh_{(n+1)}}) \tag{2}$$

$$\dot{\mathbf{u}}_{n+1} = \dot{\mathbf{u}}_n + \frac{\Delta t}{2}(\ddot{\mathbf{u}}_n + \ddot{\mathbf{u}}_{n+1}) \tag{3}$$

where Δt denotes the time step, $\mathbf{M}$ is the lumped mass matrix, $\mathbf{F}$ is the external force vector, $\mathbf{R}_{int}$ and $\mathbf{R}_{coh}$ are the global internal and cohesive force vectors, which are obtained from the contribution of *bulk* and *cohesive* elements, respectively. Large deformation formulation is employed[6].

To treat the material nonhomogeneity inherent in the problem, *graded elements*, which incorporate the material property gradient at the element level, are introduced. In this investigation, the scheme proposed by Kim and Paulino[7] is adopted. The same shape functions are used to interpolate the unknown displacements, the geometry, and the material parameters, and thus the interpolations for material properties (E, ν, ρ) are given by

$$E = \sum_{i=1}^{m} N_i \; E_i, \qquad \nu = \sum_{i=1}^{m} N_i \; \nu_i, \qquad \rho = \sum_{i=1}^{m} N_i \; \rho_i \tag{4}$$

where N_i are the standard shape functions.

3 INTRINSIC AND EXTRINSIC COHESIVE ZONE MODELS

The distinction between intrinsic and extrinsic CZMs is the presence of initial elastic curve, as shown in Fig. 3. The two models were proposed by Geubelle and Baylor[5] (Fig. 3 (a)) and Camacho and Ortiz' model[4] (Fig. 3 (b)), respectively. Intrinsic CZMs assume that, *e.g.* in pure tension case, traction T_n first increases with increasing interfacial separation Δ_n, reaches a maximum value T_n^{max}, then decreases and finally vanishes at a characteristic separation value δ_n, where complete decohesion is assumed to occur. On the other hand, extrinsic CZMs assume that separation only occurs when interfacial traction reaches the finite strength T_n^{max}, and once the separation occurs, the interfacial cohesion force monotonically decreases as separation increases.

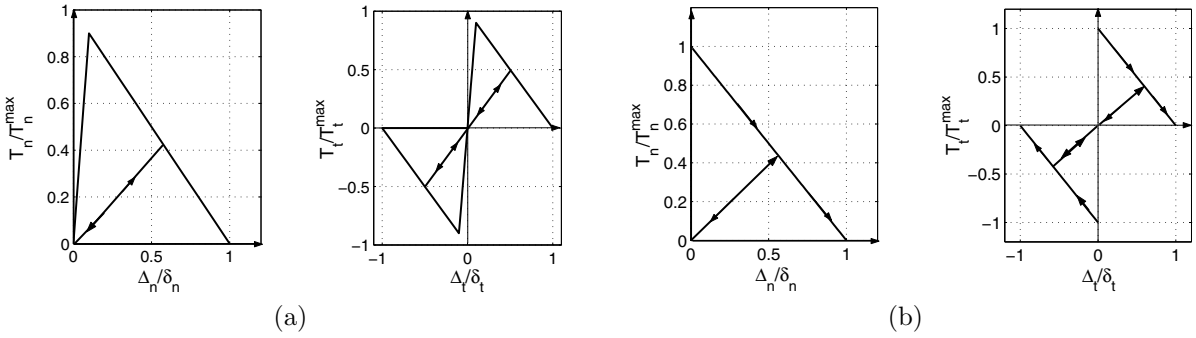

Fig. 2: Comparison of two typical intrinsic and extrinsic CZMs: (a) bilinear intrinsic cohesive zone model[3] in pure tension and pure shear; (b) initially-rigid extrinsic cohesive zone model[4] in pure tension and pure shear.

Comparison of the two types of CZMs are briefly summarized as follows:

- *Intrinsic* model requires that all cohesive elements be embedded in the discretized structure at the beginning of simulation, and the mesh connectivity remains unchanged during the whole simulation process.
- *Intrinsic* model allows easy implementation, however, it introduces artificial compliance depending on the area of cohesive element surfaces introduced and the cohesive element property. If the crack grows along a pre-defined path, the adverse effect is relatively minor, while for simulations involving cohesive element inserted in a large area, the result can be highly non-convergent for different mesh discretizations. Moreover, this concern usually necessitates adoption of very high cohesive strength, e.g., $T_n^{max} = E/10$, which is not physical.
- For *extrinsic* model, cohesive elements are adaptively inserted into the mesh. This usually requires complicated updating scheme for the modified mesh by renumbering nodes and elements.
- *Extrinsic* model avoids the artificial softening effect present in intrinsic models. The critical fracture stress adopted is usually much lower than that used in intrinsic models. For example, in their work, Camacho and Ortiz[4] used a value around $T_n^{max} = E/600$.

The above observations are made in general regarding the *intrinsic* and *extrinsic* models, not only confined to the two models illustrated in Fig 3. Different types of CZMs within each group are developed based on various considerations, and one may have certain advantage over the other for specific problems. For example, the above bilinear CZM has an adjustable initial slope, which provides the user more control on the artificial compliance than a model with fixed initial slope. Some of these issues were addressed in more detail in the work by the authors[6], where mesh convergence study was carried out for both cracks along pre-defined path and cracks along arbitrary path.

4 COHESIVE ZONE MODEL FOR FGMS

We propose a new FGM cohesive zone model[6], which is a combination of the models by Xu and Needleman[3] and Jin *et al.*[8]. It avoids effective quantities and thus uses the actual quantities to describe the relationship between normal traction-separation and tangential traction-separation.

Assume that the energy potential of each individual material phase takes the exponential form[3]:

$$\phi_i(\boldsymbol{\Delta}) = \phi_{ni} + \phi_{ni}\exp\left(-\frac{\Delta_n}{\delta_{ni}}\right)\left\{\left[1 - r_i + \frac{\Delta_n}{\delta_{ni}}\right]\frac{(1-q_i)}{(r_i-1)} - \left[q_i + \frac{(r_i-q_i)}{(r_i-1)}\frac{\Delta_n}{\delta_{ni}}\right]\exp(-\frac{\Delta_t^2}{\delta_{ti}^2})\right\} \quad (5)$$

in which superscripts i $(i = 1, 2)$ denote the two individual material phases ($e.g.$, metal and ceramic respectively), and parameters $\boldsymbol{\Delta} = [\Delta_n, \Delta_t]$ denote the displacement jump across the cohesive surface in normal and tangential directions. Other parameters in the expressions that respectively refer to material phase i are explained hereby without subscript notation: parameters ϕ_n and ϕ_t are the energies required for pure normal and tangential separation, respectively; δ_n and δ_t are the critical opening displacement for normal and tangential separation, which are related to the cohesive normal strength $T_n^{\max}$ and tangential strength $T_t^{\max}$ as

$$\phi_n = eT_n^{\max}\delta_n, \qquad \phi_t = \sqrt{e/2}T_t^{\max}\delta_t, \quad (6)$$

where $q = \phi_t/\phi_n$, and r is defined as the value of Δ_n/δ_n after complete shear separation with $T_n = 0$.

The cohesive traction force vectors associated with material phases 1 and 2 in the 2-D case comprise traction in normal and tangential directions as $\mathbf{T}_1 = [T_{n1}, T_{t1}]$, $\mathbf{T}_2 = [T_{n2}, T_{t2}]$, and can be derived directly from the energy potentials as

$$\mathbf{T}_1 = -\partial\phi_1/\partial\boldsymbol{\Delta}, \qquad \mathbf{T}_2 = -\partial\phi_2/\partial\boldsymbol{\Delta}. \quad (7)$$

The resulting normal and shear traction components are illustrated in Figure 3 (a).

Let $\mathbf{T}_{\mathrm{FGM}} = \left[T_n^{\mathrm{FGM}}, T_t^{\mathrm{FGM}}\right]$ denote the traction force vector across the cohesive surfaces of a two-phase FGM, which comprises normal and tangential traction force components. The cohesive traction $\mathbf{T}_{\mathrm{FGM}}$ is approximated by the following volume fraction based formula

$$\mathbf{T}_{\mathrm{FGM}}(\mathbf{x}) = \frac{V_1(\mathbf{x})}{V_1(\mathbf{x}) + \beta_1[1 - V_1(\mathbf{x})]}\mathbf{T}_1 + \frac{1 - V_1(\mathbf{x})}{1 - V_1(\mathbf{x}) + \beta_2 V_1(\mathbf{x})}\mathbf{T}_2 \quad (8)$$

where the parameter $V_1(\mathbf{x})$ denotes volume fraction of the material phase 1, while β_1 and β_2 are two cohesive gradation parameters that describe the transition of failure mechanisms from pure material phase 1 to pure material phase 2, and should be calibrated with experimental data. Figure 3 (b) compares the normal traction-separation laws for two material constituents.

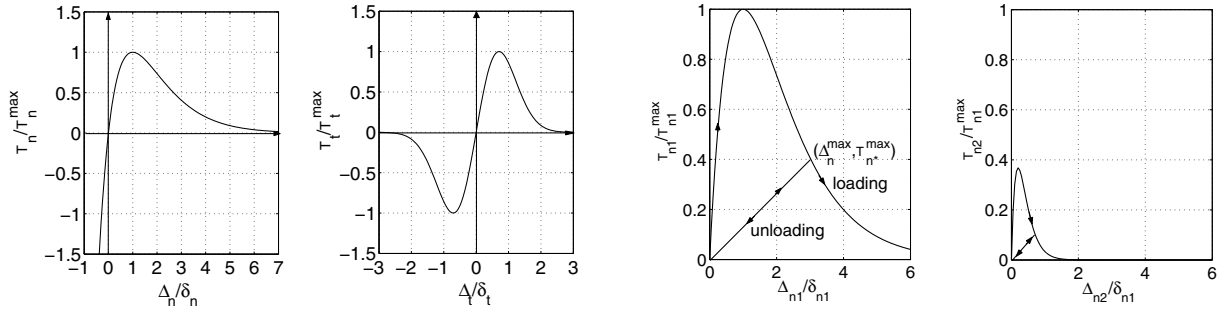

(a) (b)

Fig. 3: (a) Exponential cohesive zone model[3] in pure tension and pure shear; (b) cohesive zone model in pure tension case, for two material phases with strength ratio $T_{n2}^{max}/T_{n1}^{max} = 0.35$, and critical displacement ratio $\delta_{n2}/\delta_{n1} = 0.15$, where δ_{ni} denotes normal separation at peak normal traction for material i.

5 NUMERICAL EXAMPLE

In this section, a test example is provided to illustrate the application of the cohesive model introduced above to both homogeneous and FGM systems through investigation of dynamic crack branching phenomenon for a plane strain plate containing an initial central crack subjected to tensile velocity loading.

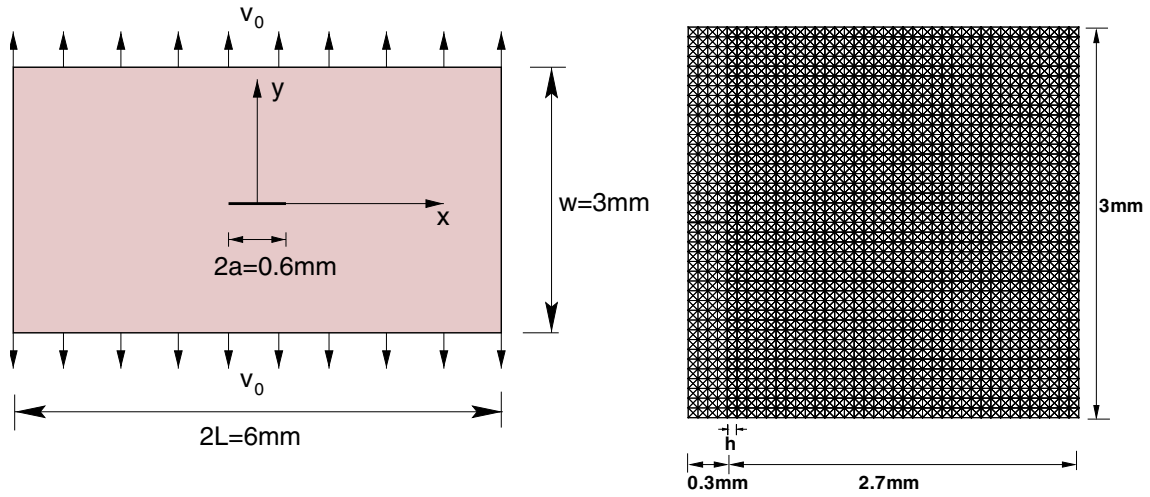

(a) (b)

Fig. 4: Branching problem; (a) geometry and boundary conditions of a plate containing a central crack subjected to velocity loading; (b) Mesh descretization of the dynamic branching problem with half of the original geometry modelled due to symmetry along the y axis.

5.1 Problem Description

The computation is carried out for a center cracked rectangular plate as shown in Figure 4 (a). Symmetric velocity loading $v_0 = 5m/s$ is applied along the upper and lower surfaces. To explore the influence of material gradation on crack branching patterns, three material gradation profiles are studied, as listed in Table 1: *case 1*: both the bulk and cohesive properties are considered for homogeneous materials; *case 2*: hypothetical "FGM", with homogeneous bulk material and linearly graded cohesive properties along y direction. *case 3*: FGM with both the bulk and cohesive properties linearly graded in y direction.

Due to symmetry of the geometry, material gradation and loading condition with respect to y axis, only the right half of the geometry is modelled for the numerical simulation, along with proper boundary condition to account for the symmetry at $x = 0$. The domain is discretized with 40 by 40 quads each divided into 4 T3 elements, as depicted in Figure 4 (b). Cohesive elements are inserted inside a rectangular region right to the initial crack, as shown with the thicker lines. The other material parameters for the CZM are: $q = 1, r = 0, and\ \beta_1 = \beta_2 = 1$.

Table 1: Three material gradation profiles for plate containing central crack.

	y position	E (GPa)	ν	ρ (kg/m^3)	G_{Ic} (N/m)	$T_{\max}$ (MPa)	δ_c (μm)
case 1: homog.	$-1/2W$ to $1/2W$	3.24	0.35	1190	352.3	324	0.4
case 2: graded T_{max}	$1/2W$	3.24	0.35	1190	528.4	486	0.4
	$-1/2W$	3.24	0.35	1190	176.1	162	0.4
case 3: graded E & T_{max}	$1/2W$	4.86	0.35	1190	528.4	486	0.4
	$-1/2W$	1.62	0.35	1190	176.1	162	0.4

5.2 Results for Various Material Gradation Profiles

Case 1: homogeneous PMMA material. Symmetric branch pattern is obtained (Figure 5 (a)). The crack begins to branch at $a_{branch} = 1.05mm$, and further branches occur when the cracks approach the edge. Although crack branching can only take place either parallel to the coordinate axes or at $\pm 45°$, the overall branching angle is less than $45°$ from the x axis. In the example, the overall branching angle is about $29°$, calculated by approximating the main branch as a straight line.

Case 2: Variation of cohesive strength. In this example, the cohesive strength T_{max} is lower at the bottom surface and higher at the top surface, which means weaker fracture resistance at the lower region. Therefore, the crack branching is expected to be more significant at the lower part of the plate, as

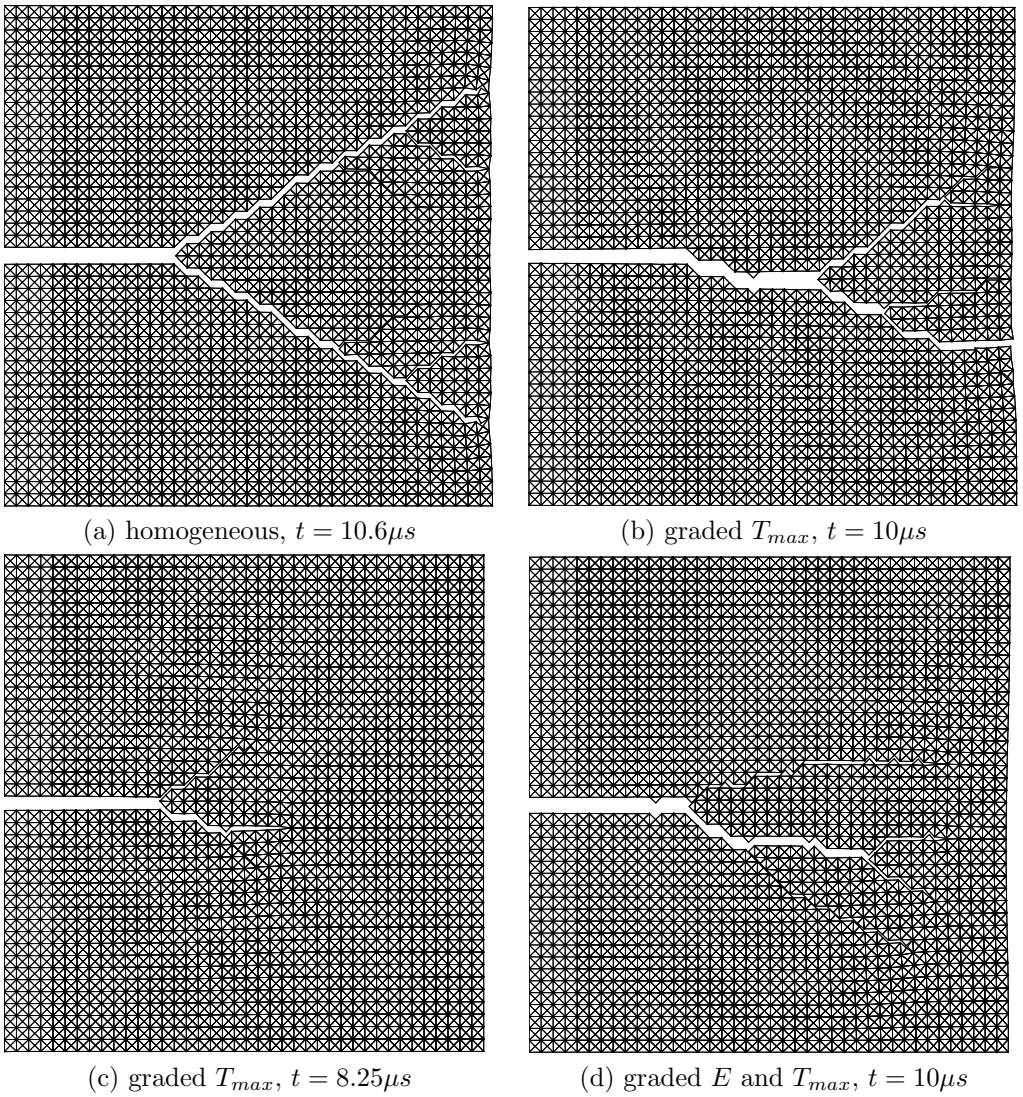

(a) homogeneous, $t = 10.6\mu s$ (b) graded T_{max}, $t = 10\mu s$

(c) graded T_{max}, $t = 8.25\mu s$ (d) graded E and T_{max}, $t = 10\mu s$

Fig. 5: Crack branch pattern for various material gradation profiles; loading velocity at $v_0 = 5m/s$; (a) final crack pattern at $t = 10.6\mu s$ for homogeneous plate (case 1); (b) final crack pattern at $t = 10\mu s$ for graded plate (case 2); (c) attempted crack branching at $t = 8.25\mu s$ for graded plate (case 2); (d) final crack pattern at $t = 10\mu s$ for graded plate (case 3).

shown in Figure 5(b). The initial crack branching location is roughly the same as the homogeneous case (Figure 5(c)), yet it disappears in the final figure (Figure 5(b)). As the lower region of the plate is weaker in resisting fracture, the crack branch towards the lower region dominates, and shields the upward one from developing further.

Case 3: Graded bulk and cohesive properties. In this example, both bulk and cohesive properties vary linearly in y direction. On one hand, the weaker cohesive resistance favors the crack branching into the $y < 0$ region. On the other hand, stress developed in the stiffer region ($y > 0$) is higher than that at the compliant region, which may promote the crack branching into the $y > 0$ region. These two mechanisms compete with each other in influencing crack branching pattern. The final crack pattern is plotted in Figure 5 (d).

6 CONCLUSIONS

This paper presents a numerical scheme incorporating CZM to investigate dynamic fracture behavior of homogeneous and FGMs under dynamic loading. Two basic types of elements are employed in the present investigation: *graded* elements in the bulk material, and *graded intrinsic cohesive* elements to model fracture. Discussion on the *pros* and *cons* of the *intrinsic* and *extrinsic* CZMs are also presented.

Xu and Needleman[3] model was extended to treat FGMs, which eliminates the dependence upon effective quantities, and may provide certain advantages when mixed-mode effect is prominent.

As illustrated in the study, the cohesive element approach is promising for modeling generalized fracture without predefined external fracture criteria. Further numerical issues, including the artificial compliance introduced in the system by incorporating cohesive elements, are studied and related results are reported in recent publication by the authors[6].

REFERENCES

[1] Paulino, G.H., Jin, Z.-H., Dodds Jr., R.H. (2003), *Failure of Functionally Graded Materials", Encyclopedia of Comprehensive Structural Integrity*, Ed Karihaloo, B. et al. Elsevier, Amsterdam, 2, pp. 607-644.

[2] Erdogan, F. (1995), "Fracture mechanics of functionally graded materials", Composites Engineering 5, pp.753-770.

[3] Xu, X. and Needleman, A. (1995), "Numerical simulations of dynamic crack growth along an interface", International Journal of Fracture 74, pp. 289-324.

[4] Camacho, G. T. and Ortiz, M. (1996), "Computational modeling of impact damage in brittle materials", International Journal of Solids and Structures 33, pp. 2899-2938.

[5] Geubelle, P.H. and Baylor, J. (1998) "Impact-induced delamination of laminated composites: a 2D simulation", Composites Part B Engineering 29, pp. 589-602.

[6] Zhang, Z. and Paulino, G. H. (2005), "Cohesive zone modeling of dynamic failure in homogeneous and functionally graded materials", International Journal of Plasticity 21, pp. 1195-1254.

[7] Kim, J.H. and Paulino, G. H. (2002), "Isoparametric graded finite elements for nonhomogeneous isotropic and orthotropic materials" ASME Journal of Applied Mechanics, 69, pp. 502-514.

[8] Jin, Z.-H., Paulino, G.H. and Dodds Jr., R.H. (2002), "Finite element investigation of quasi-static crack growth in functionally graded materials using a novel cohesive zone fracture model". ASME Journal of Applied Mechanics, 69, pp. 370-379.